Creating an Eccentric Nuclear Disk of Stars with Two Black Holes

College of Arts and Sciences Honors Thesis

Defense Date: November 3, 2021

Allie Christensen

Honors thesis committee:

Dr. Ann-Marie Madigan,

JILA and Department of Astrophysical and Planetary Sciences, CU Boulder

Dr. Seth Hornstein

Department of Astrophysical and Planetary Sciences, CU Boulder

Dr. Jamie Nagle

Department of Physics, CU Boulder

Draft version November 7, 2021
Typeset using LaTeX default style in AASTeX631

Creating an Eccentric Nuclear Disk of Stars with Two Black Holes

Allie Christensen[1]

[1] *JILA and Department of Astrophysical and Planetary Sciences, CU Boulder, Boulder, CO 80309, USA*

ABSTRACT

The Andromeda galaxy (M31) hosts a peculiar nucleus. The stars in M31's galactic center swirl about a super-massive black hole on aligned, elongated orbits – a structure called an eccentric nuclear disk. Hubble Space Telescope observations indicate that up to twenty percent of nearby galaxies exhibit features consistent with eccentric nuclear disks. Scientists remain unsure, however, of how eccentric nuclear disks form. This paper explores a new theoretical idea that an eccentric nuclear disk can form during the merger of two galaxies when two black holes inspiral towards each other. Our theory is motivated by earlier work from Thomasson et al. (1989) which showed the development of asymmetries in galactic disks when encountering large companions, and here we apply similar dynamics to galactic nuclei. We present analytic calculations and use the open source N-body integrator `REBOUND` to model the gravitational interaction between two black holes, one of which has a circular stellar disk. We find that an eccentric nuclear disk forms when the precession period of the stellar disk is in resonance with the orbital period of the black hole companion.

Keywords: Astrodynamics - N-body problem - Galactic nuclei

1. INTRODUCTION

Our neighboring galaxy, the Andromeda Galaxy, challenged astrophysicists when the Hubble Space Telescope (HST) imaged its galactic center (see Figure 1a). HST revealed a double nucleus, which Tremaine (1995) showed was due to a disk of stars on aligned, eccentric orbits; a structure called an eccentric nuclear disk (END). The two bright spots (double nucleus) seen in the image are due to the alignments of stellar apoapses and periapses. The apoapsis and periapsis correspond to the points on an orbit where a star is the farthest and closest from its central black hole. A star spends the least amount of time at periapsis as it is moving at its fastest; most of the time the star remains near apoapsis where it moves more slowly. Therefore you get two bright spots, one near the stars' unified periapsis, and a second, brighter spot near the stars' collective apoapsis where the stars spend most of their time. For a summary of how we describe orbits please refer to Appendix A.

Despite observational limitations in resolving galactic nuclei, an imaging survey of local massive galaxies by Lauer et al. (2005) suggests that up to twenty percent of galaxies show features consistent with eccentric nuclear disks (Figure 2a). Generally, we assume galactic centers are comprised of a disk with axisymmetric apoapses and periapses (Figure 2b). Madigan et al. (2018) explained how inter-orbit gravitational torques prevent differential precession in stellar disks, supporting the apparent abundance of ENDs. Further, Gruzinov et al. (2020) determined ENDs as one of the thermodynamical equilibrium states for stellar disks in galactic nuclei.

Working from these theories, we make use of the eccentricity vector when we want to know information about the farthest and closest points of an orbit. The eccentricity vector points from apoapsis to periapsis with its length being the scalar eccentricity of the object's orbit, or how elongated the stellar orbit is. To find the eccentricity vector, $\vec{e}$, we make use of the following:

$$\vec{e} = \frac{\vec{v} \times \vec{j}}{GM} - \hat{r} \ .$$

This equation tells us that plugging in the velocity, $\vec{v}$, angular momentum $\vec{j}$, position, $\vec{r}$, vectors of the star, the gravitational constant, G, and the central object (in this paper a black hole)'s mass, M_{BH}, we may derive the

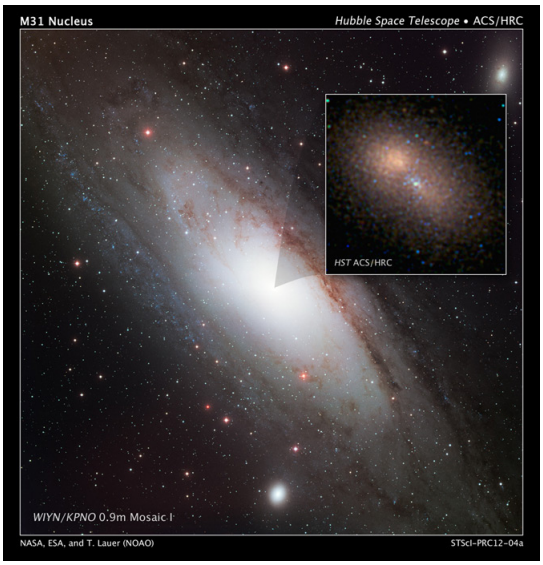

(a) M31's double nucleus.

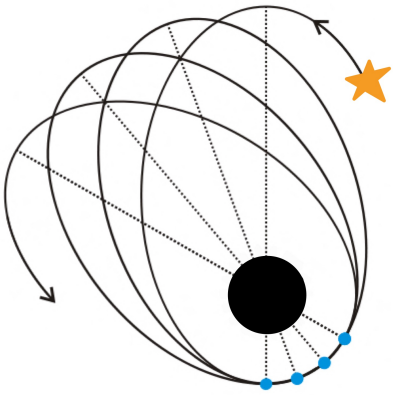

(b) Apsidal precession of an orbit.

Figure 1. (a) The Andromeda (M31) Galaxy, a Hubble (HST) image, of its double nucleus. The two bright spots (top left to bottom right), in the zoomed image, are the apoapsis and periapsis of an eccentric nuclear disk. The central super-massive black hole lies close to the smaller bright spot or the periapsis. Retrieved from Wikipedia's page on Andromeda. (b) Image showing apsidal precession of an eccentric orbit. Notice how the orbit of this star does not close every orbit, and that the orbit and precession direction are the same, so this figure shows prograde precession of a stellar orbit. Also, the apoapsis of this star's orbit swings around its black hole, and this is apsidal precession. Figure adapted from Wikipedia's page on apsidal precession.

eccentricity vector of an orbit (see Appendix A). Analysis of our stellar eccentricity vectors enable us to detect orbital precession.

Orbits in general experience precession of their stellar eccentricity vectors, that is, stellar orbits swing around their central object. Recall that eccentricity vectors describe the orientation of an orbit, and precessing orbits do not close after one orbit creating a flower looking pattern over time (Figure 1b). Objects undergoing precession

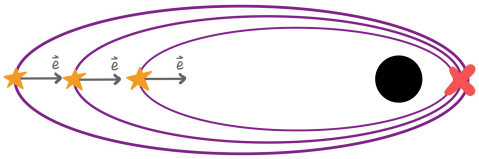

(a) An Eccentric Nuclear Disk (END).

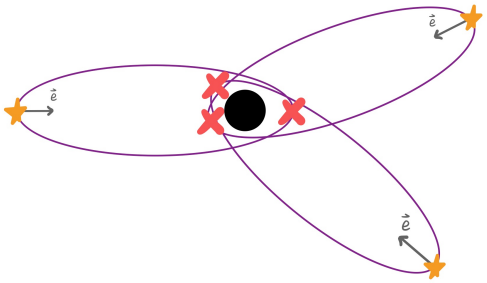

(b) Randomly oriented disk.

Figure 2. (a) Schematic of an eccentric nuclear disk (END) showing *apsidal* alignment of orbits. All the eccentricity vectors, grey arrows that point from apoapsis to periapsis, point in the same direction, so the average unit eccentricity vector would be near unity. (b) Unaligned disk, *no* apsidal alignment. The eccentricity vectors do not point in the same direction, so average unit eccentricity vector would be close to zero. Note: Diagram not to scale. The star and red 'X' represent the apoapsis (farthest point from central object) and periapsis (closest point to central object), respectively.

experience a precession rate heavily dependent upon their semi-major axis and eccentricity, so we generally expect various precession rates, or *differential precession*, across a stellar disk. Usually differential precession prevents apsidal alignment. However, in an END, inter-orbit gravitational torques change orbital eccentricities and limit differential precession (Madigan et al. 2018). For our simulations we determine a surface density profile for our stellar disk that enables us to set a uniform precession rate across every semi-major axis, and therefore limiting differential precession of the disk (see Section 2). If differential precession prevents large scale structure from forming in a stellar disk (due to randomization of orbits) then uniform precession should aid in creating disk structures.

Thomasson et al. (1989) showed that large-scale retrograde galaxy mergers – in which one galaxy orbits in the opposite direction as the other– can create a leading spiral arm in the stellar disk of the central galaxy. Formation of the leading arm results from the less massive galaxy resonating and gravitationally torquing the stellar disk, altering the orientations of stellar orbits. "Resonating" means that the stars' precession rate matches the orbital angular velocity of the companion. The companion galaxy pulls or gravitationally torques stars over time causing their orbit directions to align and precess together creating the leading spiral arm structure.

We theorize that in a system with two black holes, one of which has a circular stellar disk surrounding it (Figure 3), an eccentric nuclear disk forms if either the gravitational torque on the disk of stars is strong enough, and/or the precession rate of the stars in the disk resonate with the orbital period of the companion black hole. We run three N-body simulations, all with a thin stellar disk orbiting its central black hole, BH_1, and with some black hole companion, BH_2. We expect eccentric nuclear disks to form if the conditions, sufficient torque and/or resonance, are satisfied. If an eccentric nuclear disk forms, we could explain how a companion contributes to the formation of these lopsided

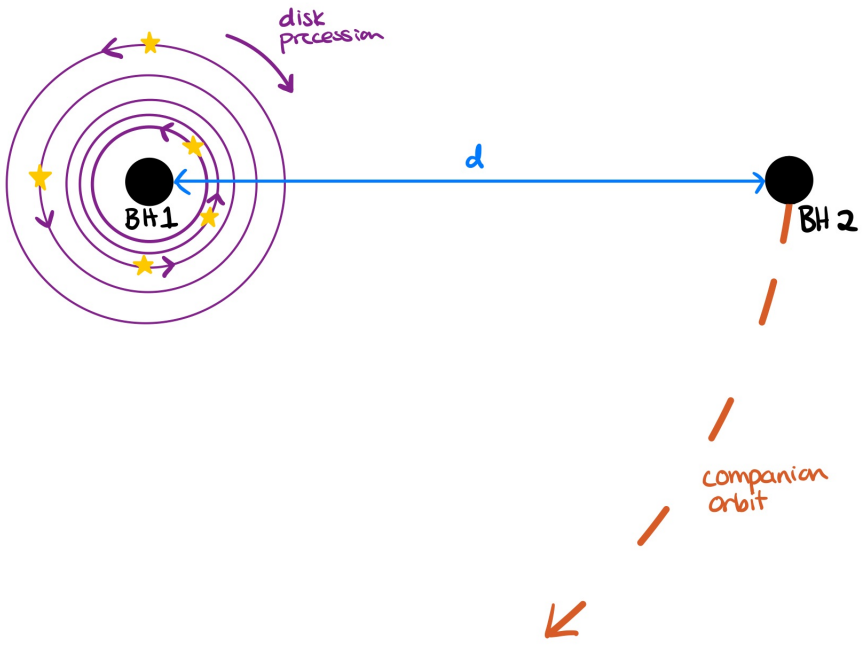

Figure 3. Schematic of our simulation setup. Our systems consist of a central black hole, BH1, with a surrbounding flat and ciruclar stellar disk that orbits counter-clockwise. The companion black hole, BH2, is a distance, "d", from BH1, and orbits BH1 clockwise. Our setup means that the disk precesses in the same direction as its companion. Note this drawing is done in the x-y plane, so the $+\hat{z}$ direction is out of the page.

disks, and then apply our formation mechanism to our neighboring galaxy Andromeda, and potentially many other galaxies showing signs of ENDs.

The rest of the thesis is outlined as follows. In Section 2 we describe the analytics of the resonant and sufficient torque conditions along with the concept of our general setup for our three cases. Next, Section 3 talks about how we initialize our `REBOUND` simulations to meet our conditions and our application of gravitational softening. We then reach our results in Section 4, where we analyze and compare plots of the unit and average unit eccentricity vectors, and orbital elements for our three simulations to check for END formation. Lastly, we get to the discussion of our results in Section 5. In our final section, we discuss which simulations form ENDs and future work.

2. ANALYTIC THEORY

Using N-body simulations alongside analytical derivations, we study the influence of three different retrograde-moving black holes around a circular disk of stars bound to the central black hole (Figure 3), but what parameters. Here we derive the black hole companion, BH2, parameters that should lead to END formation.

First, we would like the precession rate of our entire stellar disk to be independent of the semi-major axis (average distance from the central object), so that every star in the disk precesses at the same speed. A disk that precesses at the same rate can fully resonate with the motion of the companion black hole. With this constraint, we arrive at a power law distribution of semi-major axes for our stellar disk.

Then we derive the torque and resonant conditions necessary to rearrange the structure of the disk. The resonant condition gives a unique orbital period, or semi-major axis (related by Equation 1), of the companion black hole that is *equal* to the precession period of the disk. Setting the orbital precession and companion orbital period equal to one another puts the objects in a 1:1 resonance; for every one orbit BH_2 completes, the disk precesses once. Objects in resonance experience a continuous gravitational "tug" at a frequency that maximizes torque, and over time the effect will amplify stellar eccentricities. As differential precession is negligible (by design), an eccentric nuclear disk forms.

There are several equations that will be useful for us in deriving our conditions. Kepler's Third Law which in its full form is written:

$$P_{\rm orb}^2 = \frac{4\pi^2}{G(M+m)}\, a^3 \ , \tag{1}$$

where $P_{\rm orb}$ is the orbital period, M and m are the masses of the orbiter and orbitee, and a is the semi-major axis of the binary (which is roughly the distance between the orbiter and orbitee, "d" from Figure 3).

An approximate equation which relates the precession period of a body to its orbital period is given:

$$P_{\rm prec} \approx \frac{M}{M_{\rm disk\ enclosed}}\, P_{\rm orb} \ , \tag{2}$$

where $P_{\rm prec}$ is the precession period of a disk, M is the mass of the black hole (BH_1) which is assumed to be the central object around which the disk exists with a mass, M_1. Finally, $M_{\rm disk\ enclosed}$ is the mass of the disk enclosed within a certain radius. The definition of a characteristic timescale for angular momentum transfer:

$$t_J \equiv \frac{J}{\dot{J}} = \frac{J}{\tau} \ , \tag{3}$$

where t_J is the characteristic timescale, J is the angular momentum of an orbit, and τ is the torque on that orbit by some external force. In our simulation BH2 provides the external force.

Now, given these equations, we want three constraints on the system:

1. A surface density profile such that the precession period of the disk is the same everywhere.
2. The secondary black hole's (BH_2) orbital period to be equal to the precession period of the disk.
3. BH_2 is massive enough to induce enough torque on the stellar orbits to change their angular momentum within a reasonable time frame.

Let us look at these one by one.

2.1. *Surface Density Profile*

Looking at Equation 2, we note that the precession period, in general, depends on the radius of the orbit. The precession period of an approximately circular orbit at radius "a" from BH1 depends on the mass of the disk enclosed within that radius, $M_{\text{disk enclosed}}(a)$, as well as the star's orbital period at that radius, $P_{\text{orb}}(a)$, which is given by Equation 1. Our task here is to backwards-engineer a surface density profile that makes $M_{\text{disk enclosed}}(a) \propto P_{\text{orb}}(a)$ such that the precession period does not carry any a-dependence. In other words, the precession period will be constant throughout the disk for our simulations.

According to Equation 1, $P_{\text{orb}} \propto a^{3/2}$, and since we want $M_{\text{disk enclosed}}(a) \propto P_{\text{orb}}(a)$, this means that we want:

$$M_{\text{disk enclosed}}(a) \propto a^{3/2} \ .$$

If we are given some surface density profile $\Sigma(a)$, we can relate that to $M_{\text{disk enclosed}}$ by:

$$M_{\text{disk enclosed}}(a) = \int_{a_{\text{in}}}^{a} 2\pi a' \Sigma(a') \ da' \ ,$$

where a_{in} is the inner edge of the disk. Taking the derivative of both sides and solving for the surface density, $\Sigma(a)$:

$$\begin{aligned} \frac{dM_{\text{disk enclosed}}(a)}{da} &= 2\pi a \Sigma(a) \\ \implies \Sigma(a) &= \frac{1}{2\pi a} \frac{dM_{\text{disk enclosed}}(a)}{da} \ . \end{aligned}$$

Since we want $M_{\text{disk enclosed}}(a) \propto a^{3/2}$, this means that our desired surface density profile is:

$$\begin{aligned} \Sigma(a) &\propto \frac{1}{a} \frac{d}{da}(a^{3/2}) \\ \implies \Sigma(a) &\propto \frac{1}{a} \ a^{1/2} \ . \end{aligned}$$

And finally we have the power-law surface density profile that allows the whole disk to precess together limiting differential precession:

$$\Sigma(a) \propto a^{-1/2} \ . \tag{4}$$

2.2. *Resonance Condition*

Next, we focus on the resonance condition. Specifically, we want the precession period of the disk, which is now constant, thanks to our work in Section 2.1, to be equal to the orbital period of the BH_1-BH_2 system. First, let us get an expression for the precession period of the disk. This is most easily calculated at the outer edge of the disk, since at that point, $M_{\text{disk enclosed}} = M_{\text{disk total}}$, where $M_{\text{disk total}}$ is the total mass of the disk, and M_1 is the mass of our central object, BH1. If we label the outer edge of the disk is a_{out}, we can use Equation 2 to get:

$$P_{\text{prec}} = \frac{M_1}{M_{\text{disk total}}} \ P_{\text{orb}}(a_{\text{out}}) \ .$$

Using Equation 1 for $P_{\text{orb}}(a_{\text{out}})$:

$$P_{\text{prec}} = \frac{M_1}{M_{\text{disk total}}} \ \left(\frac{4\pi^2}{GM_1} \ a_{\text{out}}^3 \right)^{1/2} \ ,$$

where we have made the assumption that M_1, mass of BH1, is much larger than the mass of the star, so that $M_1 + m \approx M_1$. Simplifying, we have the precession period of the disk:

$$P_{\text{prec}}^2 = \frac{4\pi^2 M_1}{GM_{\text{disk total}}^2} \ a_{\text{out}}^3 \ . \tag{5}$$

Recalling, "d" as the separation between the two black holes, we now find the orbital period of the BH_1-BH_2 system. Again, given by Equation 1:

$$P_{\rm orb}^2 = \frac{4\pi^2}{G(M_1+M_2)}\ d^3\ . \tag{6}$$

Equating the two periods from Equations 5 and 6:

$$\frac{4\pi^2 M_1}{GM_{\rm disk\ total}^2}\ a_{\rm out}^3 = \frac{4\pi^2}{G(M_1+M_2)}\ d^3\ .$$

After cancellations and simplifications, we obtain the equation for our resonance condition:

$$\frac{a_{\rm out}^3}{d^3} = \frac{M_{\rm disk\ total}^2}{M_1(M_1+M_2)}\ . \tag{7}$$

2.3. *Torque Condition*

Finally, we look at the third constraint that states the external force from BH_2 must induce enough torque to change the angular momentum of a stellar orbit within a reasonable time frame. We would like what defines a reasonable time frame to be quite flexible, so let us say that this is some multiple of the orbital period of the star, $nP_{\rm orb}$. Then it seems reasonable to set our characteristic timescale, defined by Equation 3, to be equal to some multiple of the orbital period:

$$t_J = \frac{J}{\tau} = nP_{\rm orb}\ .$$

Here, J is the magnitude of the angular momentum of the stellar orbit. For a circular orbit at some radius $a_{\rm star}$, this is:

$$\begin{aligned} J &= |m\vec{r}\times\vec{v}| \\ &= ma_{\rm star}\sqrt{\frac{GM_1}{a_{\rm star}}} \\ &= m\sqrt{GM_1\ a_{\rm star}}\ , \end{aligned}$$

where m is the mass of the star. For τ, the torque, we want to calculate the external torque on the star caused by BH_2. For an order-of-magnitude estimate, we assume $d \gg a_{\rm star}$ such that the magnitude of the gravitational force can be estimated by Newton's Law of Gravitation, $F = \frac{GM_2m}{d^2}$. Then, we simplify by assuming that $\vec{r}\perp\vec{F}$,

$$\begin{aligned} \tau &= |\vec{r}\times\vec{F}| \\ &= a_{\rm star}\frac{GM_2m}{d^2}\ . \end{aligned}$$

Next, we use Equation 1 for $P_{\rm orb}$:

$$P_{\rm orb}^2 = \frac{4\pi^2}{GM_1}\ a_{\rm star}^3\ .$$

Now, we plug in $P_{\rm orb}$, J, and τ into Equation 3:

$$\frac{m\sqrt{GM_1\ a_{\rm star}}}{a_{\rm star}\frac{GM_2m}{d^2}} = n\left(\frac{4\pi^2}{GM_1}\ a_{\rm star}^3\right)^{1/2}\ .$$

And with substantial simplification we obtain the condition of sufficient torque:

$$\frac{M_1}{M_2} = 2\pi n\frac{a_{\rm star}^2}{d^2}\ . \tag{8}$$

With this in mind, we run the three N-body simulations: one where both the resonant (Equation 7) and sufficient torque condition (Equation 8) are satisfied, one where just the torque condition is satisfied, and a simulation just meeting the resonance condition.

Simulation	Resonance	Torque	M_1	$M_{\rm disk}$	N	m	M_2	d
RT	✓	✓	1	1/100	200	5e-5	27.7	132
T		✓	1	1/500	200	1e-5	27.7	132
R	✓		1	1/500	200	1e-5	1	25.07

Table 1. Simulation Parameters. RT, the simulation that meets both the resonating and torquing conditions, T is the simulation that satisfies the torque condition, and the R simulation meets the resonance condition. Recall we initialize the central object mass, M_1, disk mass, $M_{\rm disk}$, number of stars in the disk, N, star mass, m, companion black hole mass, M_2, and the separation between the two black holes, d, to meet the resonance and sufficient torque conditions, Equations 7 and 8.

3. N-BODY SIMULATIONS

Creating our three simulations requires we utilize a software package that allows us to accurately model gravitational systems with the specifications shown in Table 1. We use `REBOUND`, an open-source, N-body simulation package with the `IAS15` integrator, a high accuracy non-symplectic integrator with adaptive time-stepping (Rein & Liu 2012; Rein & Spiegel 2015). We use code units of $G = 1$, $M_1 = 1$, and the inner edge of the disk $a_{\rm in} = 1$ such that the period of a circular orbit at the inner edge of the disk is $P(a_{\rm in}) = 2\pi$.

Then, we initialize stars in an axisymmetric, thin disk with $N = 200$ stars in the range $a = 0.9 - 2$ with surface density profile $\Sigma \propto a^{-1/2}$, stellar eccentricities of $e = 0.1$, inclination Rayleigh distributed with $\sigma = 1°$, longitude of periapsis (ϖ) and mean anomaly (time averaged true anomaly, see A) uniformly distributed in $[0 - 2\pi)$. In Table 1, we state additional companion (BH2) and disk properties initialized in our simulations.

3.1. *Gravitational Softening*

Looking again at Newton's Law of Gravitation, $F = \frac{GM_2m}{a^2}$, as perturbed objects in our simulation experience close encounters, the separation a approaches zero in the denominator and the force can go to infinity.

By setting gravitational softening to 10^{-5} – adding this value to the denominator of Newton's Law of Gravitation, $F = \frac{GmM_2}{(a+10^{-5})^2}$ – we "soften" the maximum gravitational force felt by a particle. Notably, we treat the stars in our disks as point-like, so tidal disruption, mergers, or collision events are not covered in this paper. Applying gravitational softening and parameterizing our three simulations we model our variations of the system shown in Figure 3.

4. RESULTS

To evaluate the effects of the torque and resonant conditions we start by looking at the cross-sectional plots of the stellar disks' eccentricity vectors and the evolution of average unit eccentricity vector of each disk to determine the overall alignment of orbits within the disk. We then analyze the mean Kepler elements of each disk. An eccentric nuclear disk shows clustering in its disks' eccentricity vectors (or the longitude of periapsis, ϖ) or an aligned average unit eccentricity vector, refer to Figure 2 and Appendix A for explanations of the eccentricity vector and ϖ.

In Figure 4, we plot the RT simulation's stellar eccentricity vectors every ten orbital periods of BH_2 (or the precession period of the disk), and we show the difference between the eccentricity vectors of all the bound disk compared to the eccentricity vectors made solely from stars near the inner edge of the disk. We notice in both panels that the stars posses a large range of semi-major axes compared to the initial distribution of semi-major axes [0.9,2]. Additionally, we fail to see clear apsidal alignment within the stellar disk since we do not see the eccentricity vectors sticking together as time goes on, meaning a stable eccentric nuclear disk did not form in our RT disk.

The apparent apsidal alignment, seen most clearly in the right panel, is fictitious due to a small number of particles left in the disk. The number of bound particles in the stellar disk seems to be a small fraction of the initial number of objects in our disk. Looking at the other simulation undergoing strong torques we find similar dynamics occurring in the that disk.

Figure 5 shows the evolution of eccentricity vectors of the T (torque condition) stellar disk from a top-down and side view. More stars remain bound to BH_1 compared to the RT simulation. Still, no obvious apsidal alignment exists due to the seemingly random distribution of eccentricity vectors. Notably, the star's eccentricity vectors get shoved out of the x-y plane indicating that their orbits are inclining out of the plane. More particles stay bound to BH_1 in this T

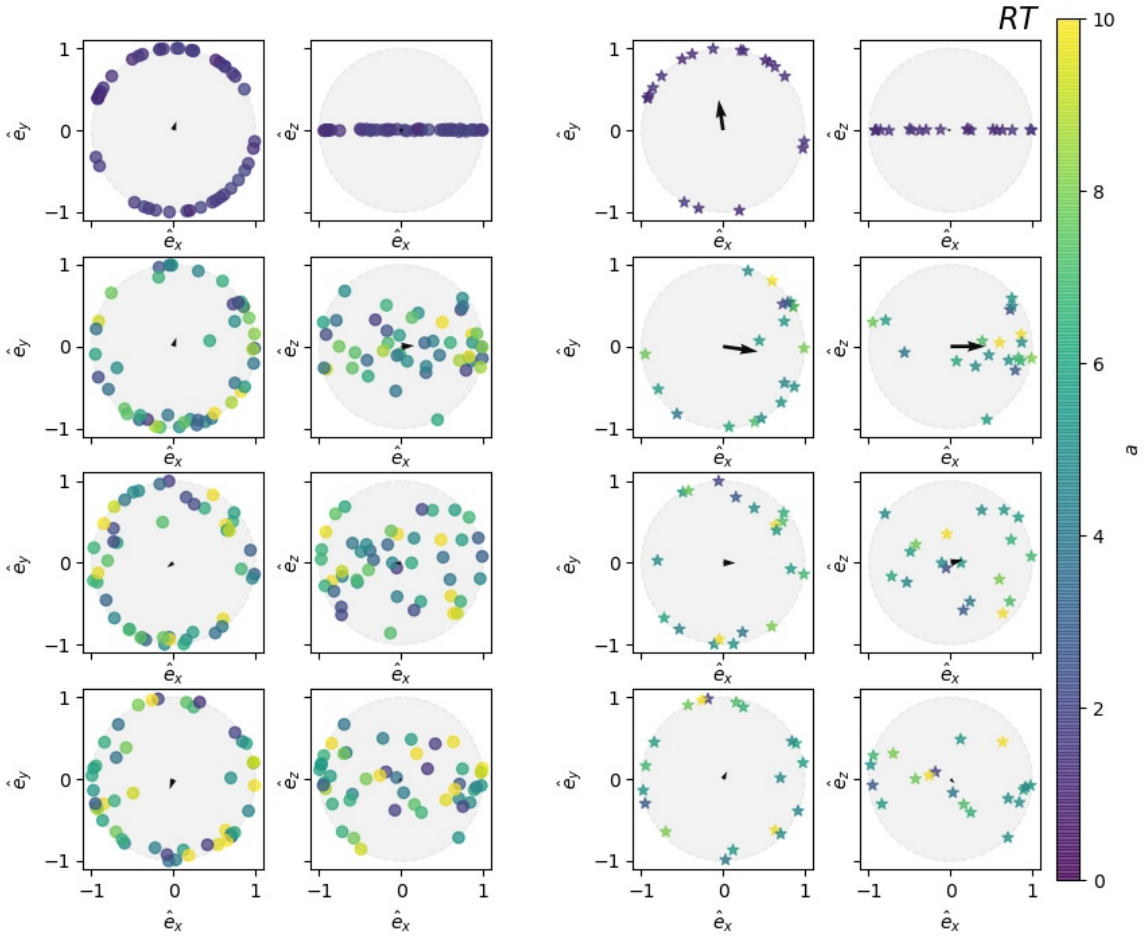

Figure 4. Evolution of each bound star's unit eccentricity vector in the RT sim. This figure shows four snapshots as rows, (t = 0, 10, 20, and 30 $P_{\mathrm{BH_2/Prec}}$) of the unit eccentricity vectors over the simulation. The two left columns show the unit eccentricity vectors of all the bound stars in the simulation (circles), and the two right columns show the unit eccentricity vectors of particles near the inner edge of the disk (semi-major axes < 1.5). With the left-most columns in both panels show a 'top-down' view of the unit eccentricity vectors, $\hat{e}_{\mathrm{y}}$ v. $\hat{e}_{\mathrm{x}}$, and the right-most columns are the 'side' view of the unit eccentricity vectors, $\hat{e}_{\mathrm{z}}$ v. $\hat{e}_{\mathrm{x}}$. The color of each symbol shows the semi-major axis of the object. The black arrows represent the average unit eccentricity vectors of the disk.

simulation, for our more massive disk (compared to RT) provides stronger inter-orbit gravitational forces requiring a star to receive a larger kick, more energy, from BH2 to unbind from its orbit.

Lastly, in Figure 4 we see the eccentricity vectors of the R (resonance condition) simulation. Again, analysis of the R cross-sectional plots for both the bound and inner disk objects reveal no apsidal alignment. We find the smallest out-of plane components of the R simulations' eccentricity vectors compared to the RT and T disks indicating we retain a relatively flat disk in the resonating case. Contrary to the RT and T simulation, we find that the R setup keeps most of its particles throughout the duration of the simulation.

With the cross-sectional eccentricity vector plots showing negative results, we analyze the evolution of the average unit eccentricity vector. Recall, clustering of the eccentricity vectors in the disk determines whether apsidal alignment exists, so disks with no or little apsidal alignment consist of random eccentricity vector orientations, Figure 2(b), but

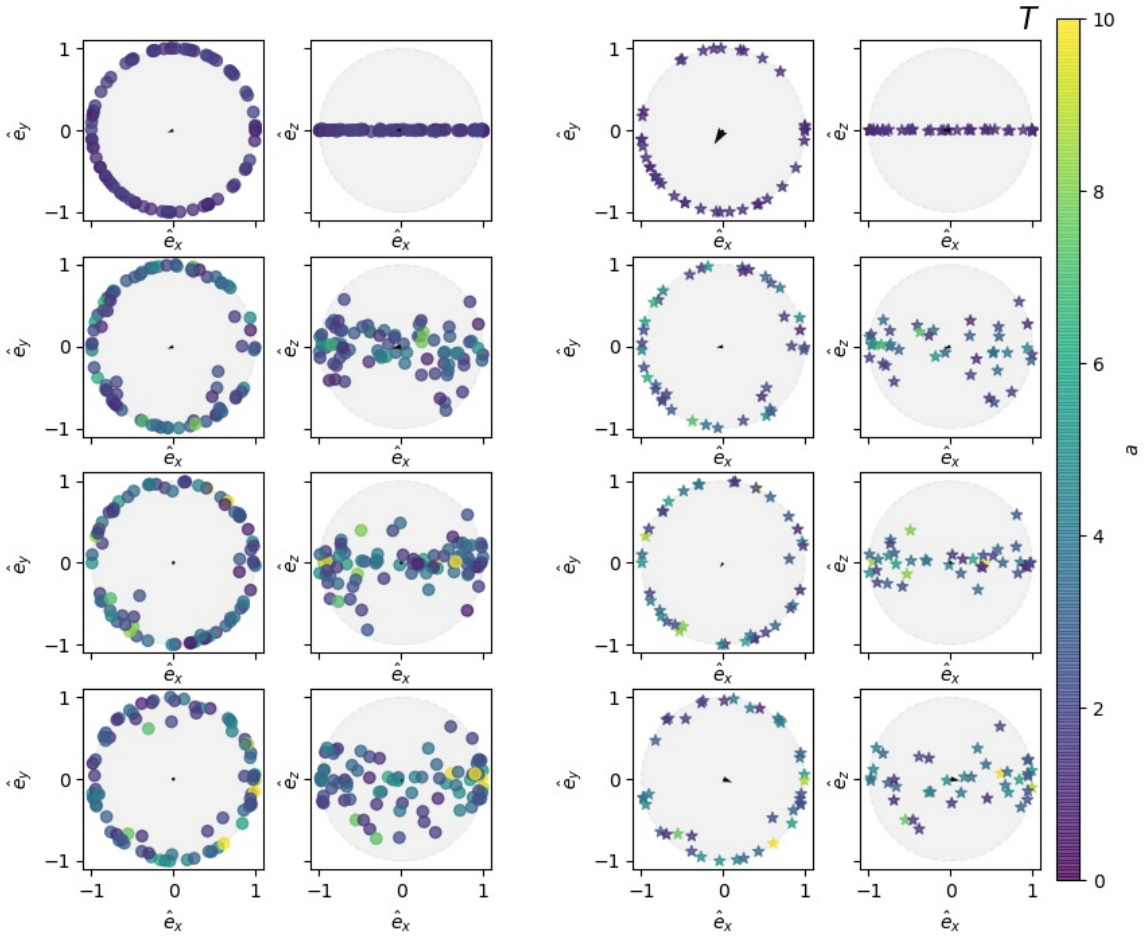

Figure 5. Evolution of each unit eccentricity vector for the stars in the T simulation. Similarly to Figure 4, these are the unit eccentricity vectors of all bounds stars in the disk, two left columns, and stars near the inner edge of the disk (semi-major axes < 1.5), two right columns. Color indicates the semi-major axis.

disks with apsidal alignment, are comprised of objects with similar orientations (or longitude of periapsis), Figure 2(a). To examine overall alignment in the disk we find the average, or normalized, unit eccentricity vector, defined as:

$$\langle \hat{e} \rangle = \sum_{n=1}^{N} \frac{\hat{e}_n}{N} \ , \tag{9}$$

where $\hat{e}_n$ is the unit eccentricity vector of star n, and N is the number of particles currently bound to BH_1. The average unit eccentricity vector for an isotropic distribution stars would approach zero, for the different orientations of each orbit provide no general direction for the overall disk orientation (Figure 2(b)). A disk with aligned eccentricity vectors would result in a normalized eccentricity vector length closer to unity (Figure 2(a)), for the similar directions of eccentricity vectors each contribute to the overall orientation of the disk. Remember that alignment of the eccentricity vectors over time means that an END formed, so ENDs return an average unit eccentricity vector that is near one, but if no END forms then the average unit eccentricity vector stays close to zero.

Plots of the average unit eccentricity vector of each simulation for the bound disk and the near resonance objects can be analyzed for apsidal alignment. First, the average unit eccentricity vector of the bound disk in each simulation barely surpasses the noise floor, $\sigma = N_{bound}^{-\frac{1}{2}}$, so no apsidal alignment of the disk occurs. Alternatively the average unit eccentricity vector for the stars near the inner edge of the disk looks noisy, but shows apparent clustering in the RT

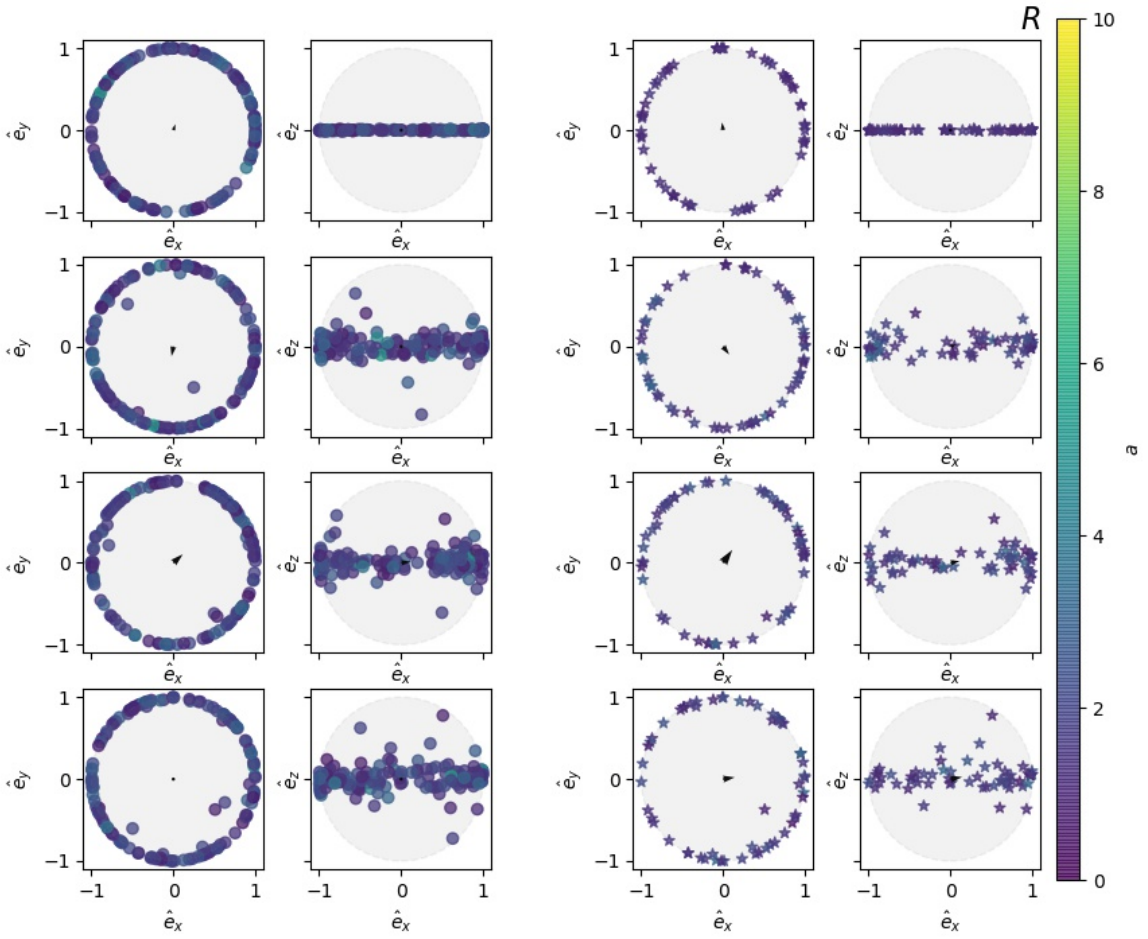

Figure 6. Evolution of each stellar unit eccentricity vector for the bound particles in R disk. Similarly to Figure 4 and 5, these are the unit eccentricity vectors of all bounds stars in the disk, two left columns, and stars near the inner edge of the disk (semi-major axes < 1.5), two right columns. Color indicates the semi-major axis.

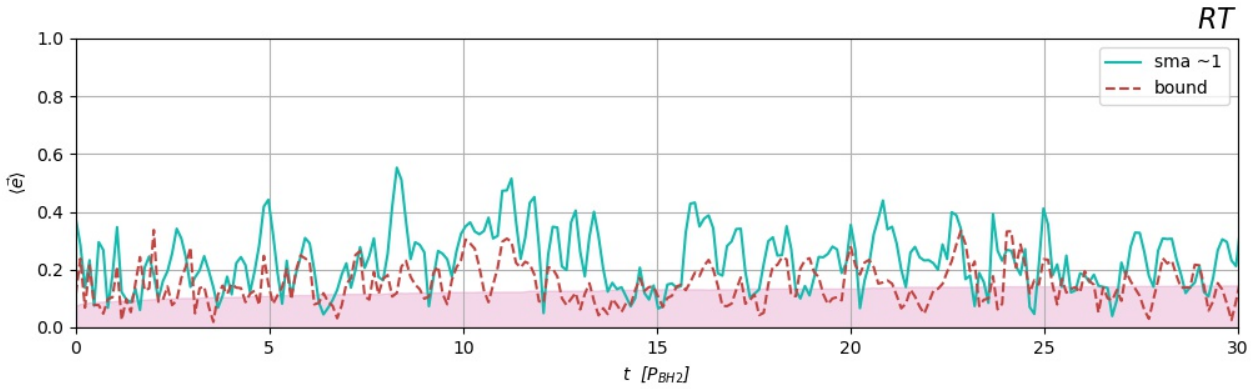

Figure 7. Evolution of the average unit eccentricity vectors of the bound stars in the disks. The y-axis shows the magnitude of the average unit eccentricity vector and the x-axis shows time. The simulation runs to thirty orbital periods of BH_2 (or orbital precession periods of the disk). The red dashed line shows the average unit eccentricity vector of all bound stars, and the solid line consists of stars near the inner edge of the disk. The pink shaded region represents the noise, $\sigma \propto \frac{1}{\sqrt{N_{bound}}}$.

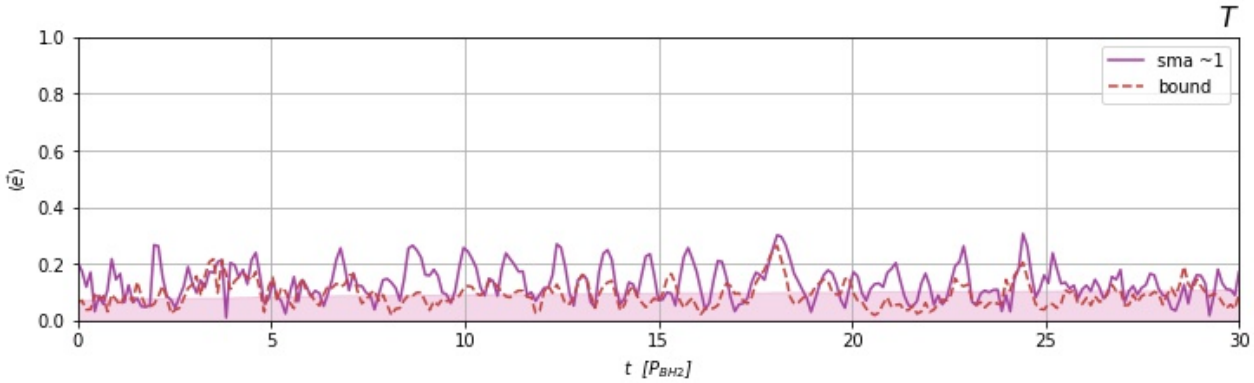

Figure 8. Evolution of the average unit eccentricity vectors of the bound stars in the disks.

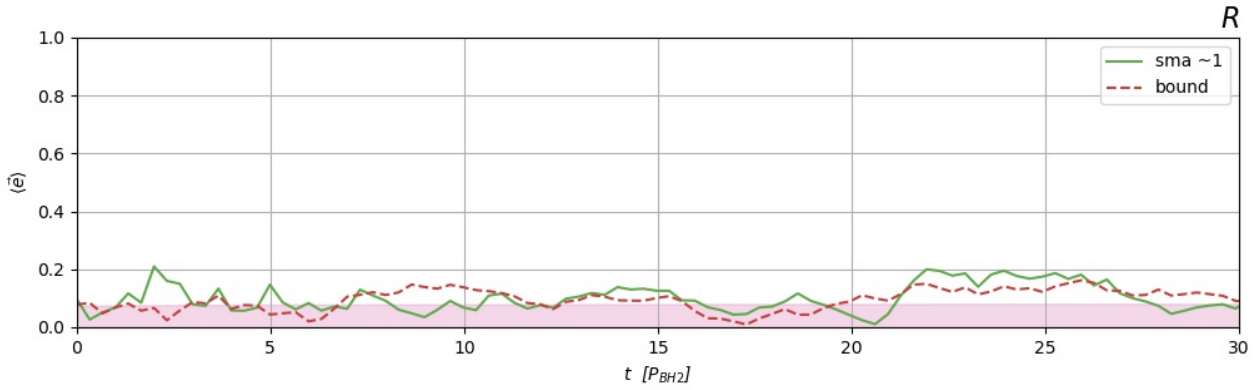

Figure 9. Evolution of the average unit eccentricity vectors of the bound stars in the R disk.

simulation, Figure 7. Similarly, the average unit eccentricity vector of the disk slightly surpasses the noise floor in the T and R disks, Figure 8 and 9, and the inner disk also shows no significant alignment.

The average unit eccentricity vector results confirm artificial alignment and apparent lack of apsidal alignment found from the corresponding Figures 5, 4, and 4. Since apsidal alignment can also be described by clustering in the longitude of periapsis, ϖ, we may see more obvious cluster of ϖ for the short timescale in which we analyze these simulations.

Figure 10 plots the average Kepler element for bound stars in the RT disk. Importantly, the eccentricity plotted here is the average eccentricity of the disk and not a sign of apsidal alignment. We see that on average the shape of the bound particles orbits' become less circular over time since the average eccentricity sits around 0.4. Also, the disks' average inclination increases during the simulation along with the average distance from BH_1, the semi-major axis. The non-uniform development of longitude of periapses, ϖ, suggests that we did not form a long lived END in the RT simulation. Comparison of our RT disk to the T disk shows similar findings.

The orbital elements of the T disk are shown in Figure 11 where we see similar dynamics shaping the disk. As in the RT simulation, we observe that average eccentricities, inclinations, and semi-major axes increase during the simulation, but with less extreme average values than measured in the RT disk. As previously mentioned, when discussing the average unit eccentricity vectors, we see less noise in the average T Kepler elements compared to the RT orbital elements. Lastly, we observe what looks to be more coherent longitude of periapses in the T disk. These orbital elements tell us that similar to the RT disk, the T disk become eccentric, puffy and spread out, but still remains more circular, flat and small compared to the RT disk. If we compare the RT and T disk average Kepler elements against

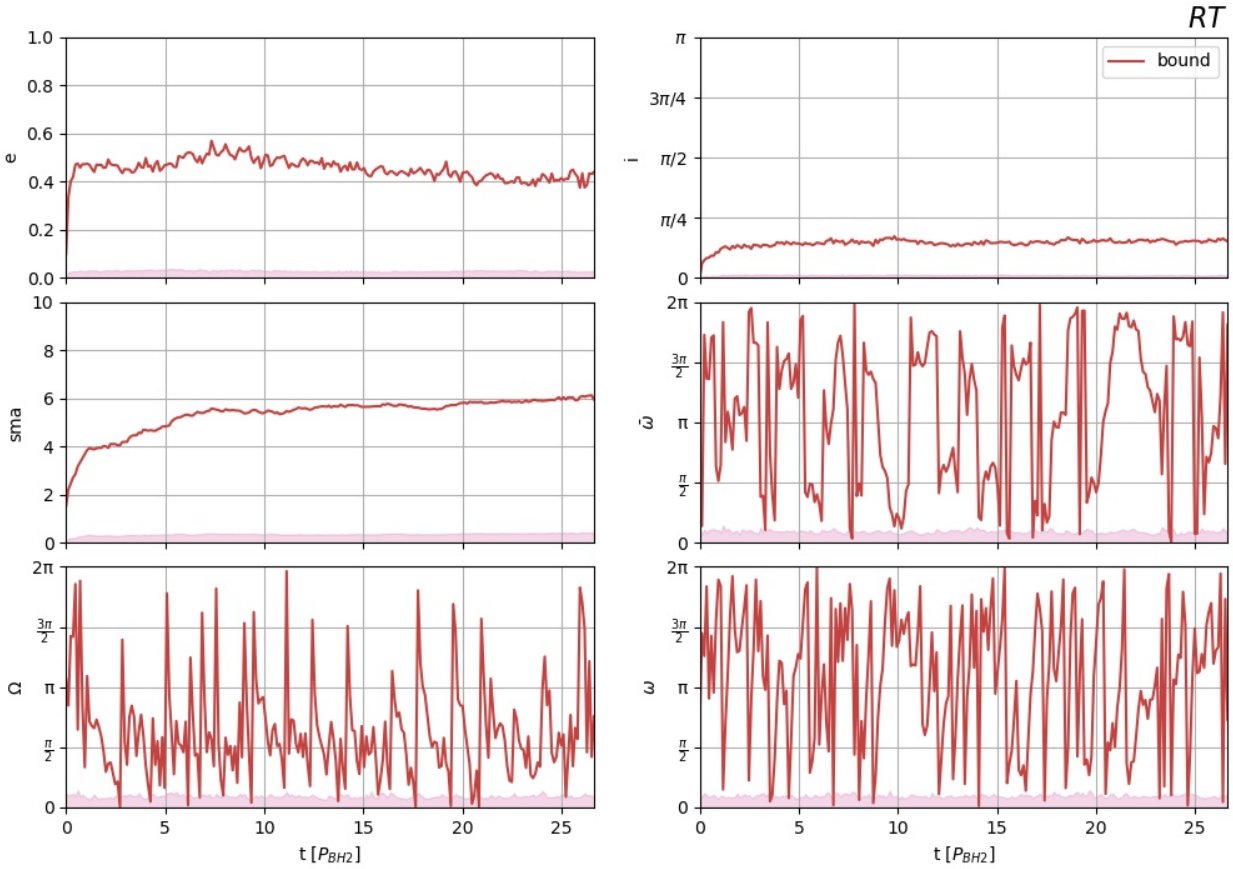

Figure 10. Average Kepler elements of the bound particles in the disk of the RT simulation. Starting from the top left plot, moving right and then down, we have the average eccentricity ('e'), inclination ('i'), semi-major axis ('sma'), longitude of periapsis ('ϖ'), longitude of ascending node ('Ω'), and argument of periapsis ('ω'). The noise floor, standard deviation of the mean, is represented by the pink shaded region.

the orbital elements for the R simulation we discover more promising results.

Observation of the previous orbital elements show a dynamical mechanism called two-body relaxation in our simulations of the RT and T disks. Conceptually, two-body relaxation is the result of star-star gravitational forces randomizing each others' orbits. This randomness means no overall alignment occurs, for star-star relaxation (two-body relaxation) spreads out the disk and slows its precession. What is happening in two-body relaxation is, stars near the outer edge of the disk get pushed past our initial outer disk edge due to gravitational encounters that change stellar energies thereby changing the their semi-major axis, and overall the star-star relaxation spreads out the disk. Two-body relaxation depends upon the number of particles in the simulation, $t_{relax} \propto N^1$ (Rauch & Tremaine 1996). In low particle sims the stars feel more extreme tugs on their orbits from the few other stars present, and this spread our disk out faster, but it is important to note that realistically galactic systems consist of *significantly* more particles than our simulations, so two-body relaxation is very slow if it affects the system at all. For scenarios like our stellar disks, we expect the semi-major axis range to increase, causing slower precession which is observed in the RT and T simulations, Figures 10 and 11, and this demonstrates that two-body relaxation contributes to the lack of apsidal alignment measured. However, star-star relaxation does not pose such a large risk for our resonating disk that is able to maintain its disk since its companion is the least massive.

The orbital elements of the R disk in Figure 12 shows the disk stay closer to our initialized values (a smaller, flatter disk), but we immediately notice dramatically different longitude of periapsis evolution for the R disk. The clear oscillations in ϖ tell us that the average orientation of the bound disk does in fact precess together despite the lack

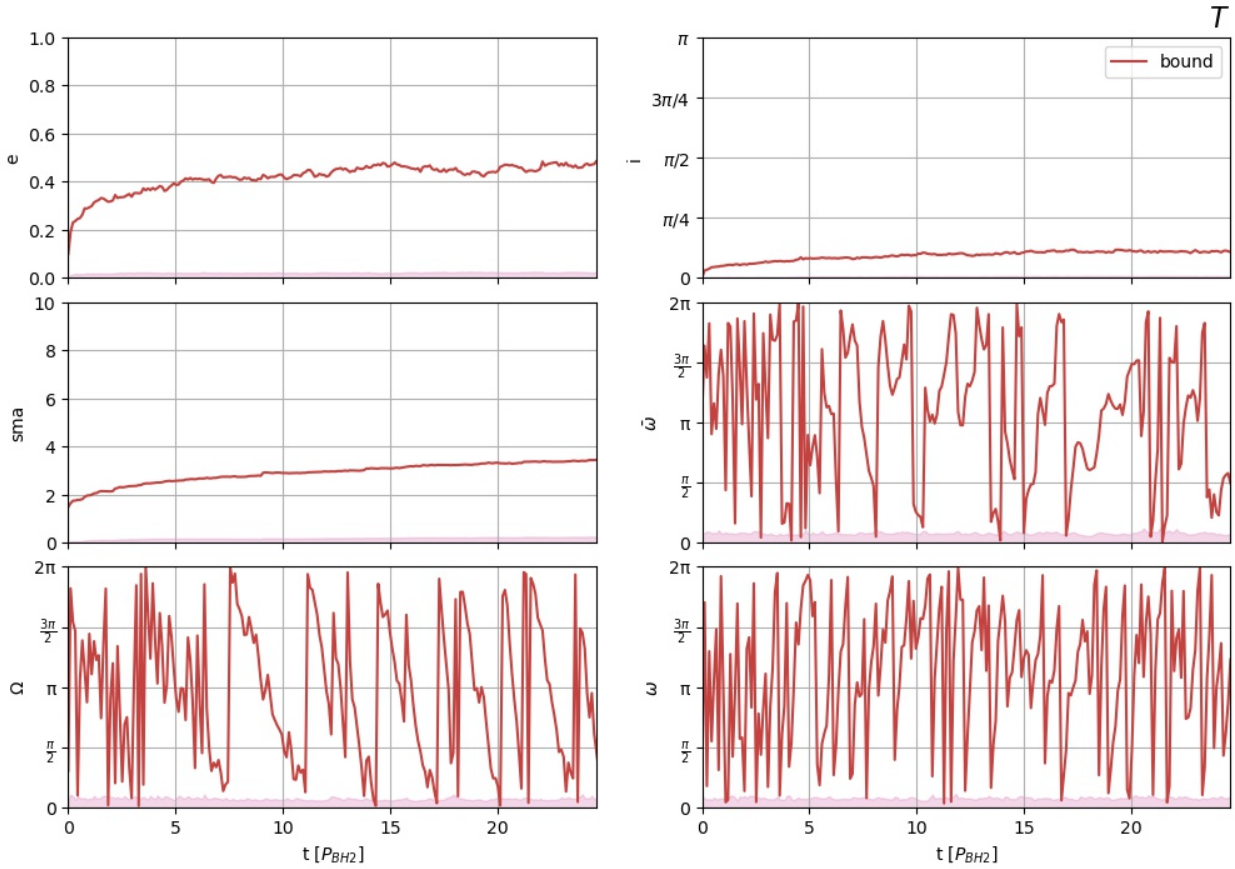

Figure 11. Average Kepler elements of the bound stars in T disk.

of apsidal alignment seen in Figures 9 and 4. Notice this simulation runs for 100 orbital periods of the companion compared to the RT and T simulations, for the R simulation forms an END! Contrary to our initial predictions, we find our R simulation displaying the most prominent signs of an END without encountering as significant dissipation of our disk due to two-body relaxation.

So far, analysis of the eccentricity vectors and orbital elements of our torquing (RT and T) stellar disks do not point to either simulation forming an END. Unexpectedly, we found that the R disk formed an END which was visible through the disks' longitude of periapsis ('ϖ') exhibiting clear oscillations in Figure 12. Notably, the noise from Figure 7 and 8, and the low number of particles in Figure 3 and 4, suggest that the number of unbound particles play a role in the evolution of our torqued simulations. Specifically for the RT and T simulations, we look into the number of unbound particles over time.

Figure 13 shows the evolution of the number of unbound particles in each disk during the simulation. We see that the torqued simulations, RT and T, lose roughly 80 and 60 percent of their disks respectively! This huge mass loss implies that the torqued disks fall out of resonance with their companion. The final M_{disk} is approximately twenty percent of its initial mass, so we expect that the precession rate of the disk no longer matches the orbital period of BH_2.

Why does this happen? Why do so many stars become unbound? Large disk mass loss is due to the extremely massive companion black hole, BH_2, in the RT and T simulations. The stars in the torqued disks feel such a strong gravitational force from their BH_2 that stars in the disk gravitationally unbind from BH_1 and escape the system. With fewer stars in the disk, the precession time increases and the disk drops out of resonance with the orbital period of BH_2. Since we did not account for the large loss of stars in the RT and T disks, we should not expect to form

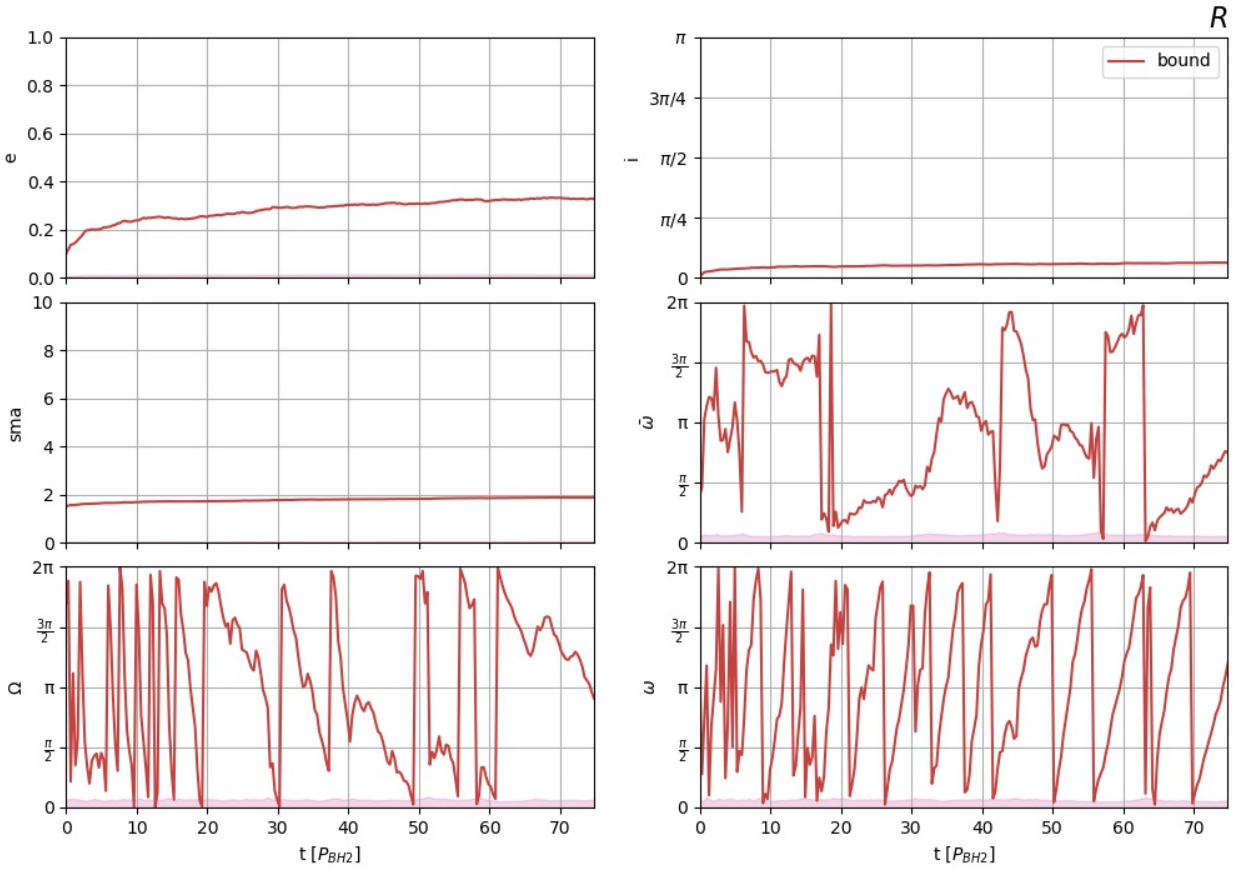

Figure 12. Average Kepler elements of the bound stars in the R disk.

ENDs. Changing precession rates means BH_2 only torques its disk, and the time in which apsidal alignment should form occurs sooner.

The effect of the strong gravitational interactions on each disk is shown through plots of an unbound star's Kepler elements, seen in Figures 14, 15, and 16, for RT, T, and R respectively. We notice that in each simulation, the soon-to-be-unbound star's orbit becomes more elliptical and precesses rapidly. For the torqued (T) simulation, we also see that the star undergoes inclinations oscillations, its semi-major axis increases, and precession of ϖ slows. Additionally, when the object becomes unbound, its eccentricity goes to infinity and its semi-major axis drops below zero, so the unbound stars gain enough energy from BH_2 to be ejected from the system entirely.

Contrary to our initial theory, the resonant (R) simulation proves to be the only system where we find evidence that an END formed. Although the eccentricity vector and average unit eccentricity vector plots do not show significant signs of apsidal alignment, we find evidence of an END in the coherent motion of the average longitude of periapsis of the disk (Figure 12).

5. DISCUSSION

This paper focuses on a scenario in which galaxy mergers, and in particular inspiraling massive black holes, form eccentric nuclear disks from initially flat, circular ones. Circular disks of stars around central black holes are expected due to gas fragmentation in gas disks, but ENDs have stayed a mystery for over twenty-five years. We show analytically that we should create an eccentric nuclear disk from a flat disk of stars due to a retrograde black hole companion inspiraling towards its counterpart, BH_1, after a galaxy merger. When the orbital period of a companion matches

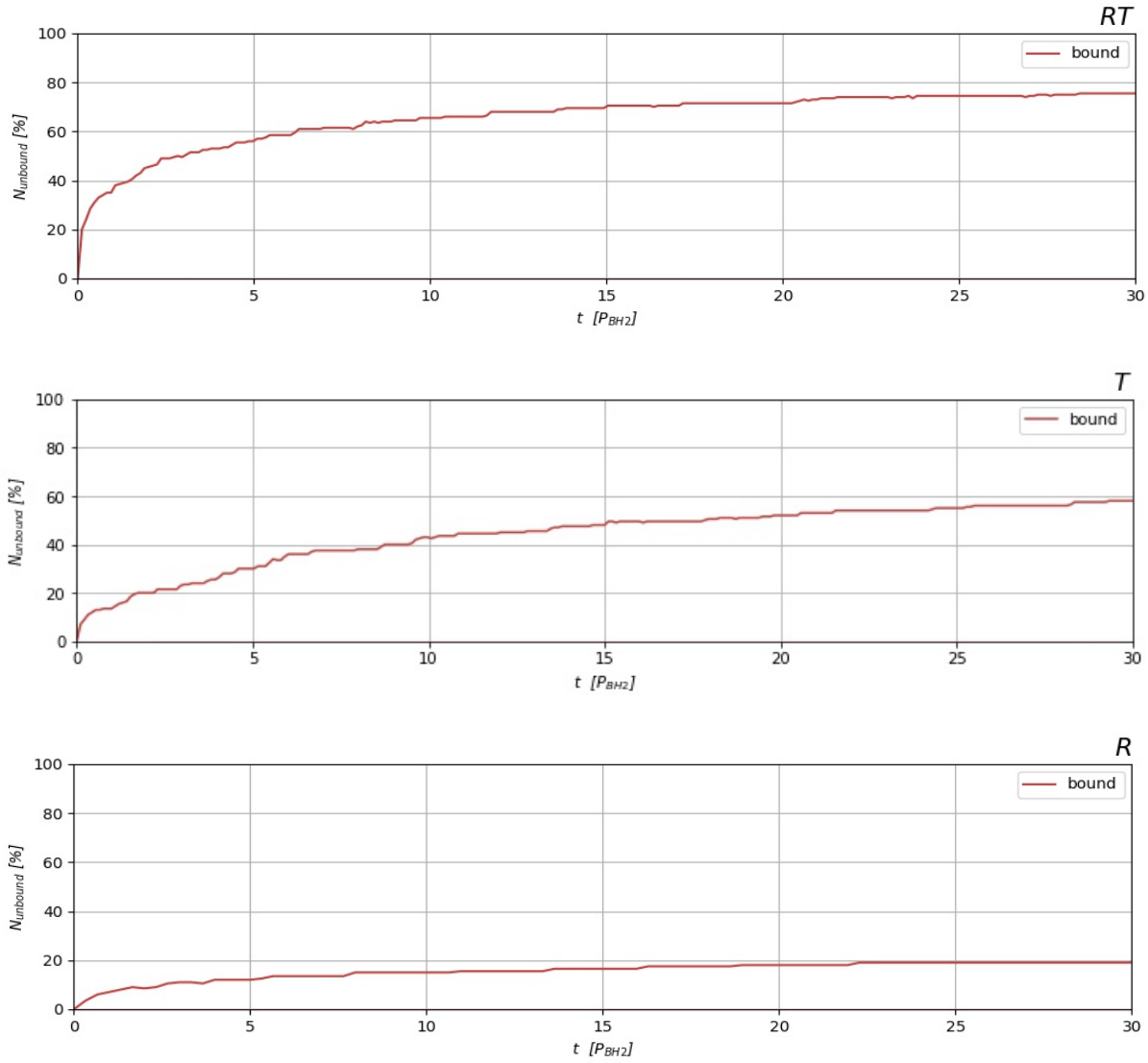

Figure 13. Percent of unbound particles for each simulation. This plot shows the percent of unbound particles, all start with N=200, for the duration of each simulation. Notice the two torqued disks show the highest percent of disk loss.

the precession period of the stellar disk, Equation 7, and the companion has enough mass to sufficiently torque the stellar orbits over a reasonable timescale, Equation 8, an eccentric nuclear disk should form. From these equations we determined the unique mass and orbital period of BH_2 needed to resonate and/or torque our flat disks so as to model the three systems (RT, T, R) through REBOUND. Analysis of our simulations showed that a black hole companion resonating with its disk aligns the eccentricity vectors in the disk resulting in oscillations of the average longitude of periapsis, Figure 12, signifying an END formed. With the RT and T data failing to show signs an END formed we examined the number of unbound stars and found that the disks were depleting in mass and dropping out of resonance.

Our work on the dynamics in a two black hole system with a stellar disk around one object encountered issues in the torqued systems that prevented END formation, but their outcomes demonstrate the importance of massive companions in our simulations. The high mass BH2s provide the stars in the disk with enough energy to escape, (become unbound from the system). A large number of particles prevents two-body relaxation from influencing our disks too strongly on the short timescales in which we observe, and large amounts of particles prevent our BH_2s from falling out of our resonance condition with our disk. Adding gravitational softening to our simulation limits the mass

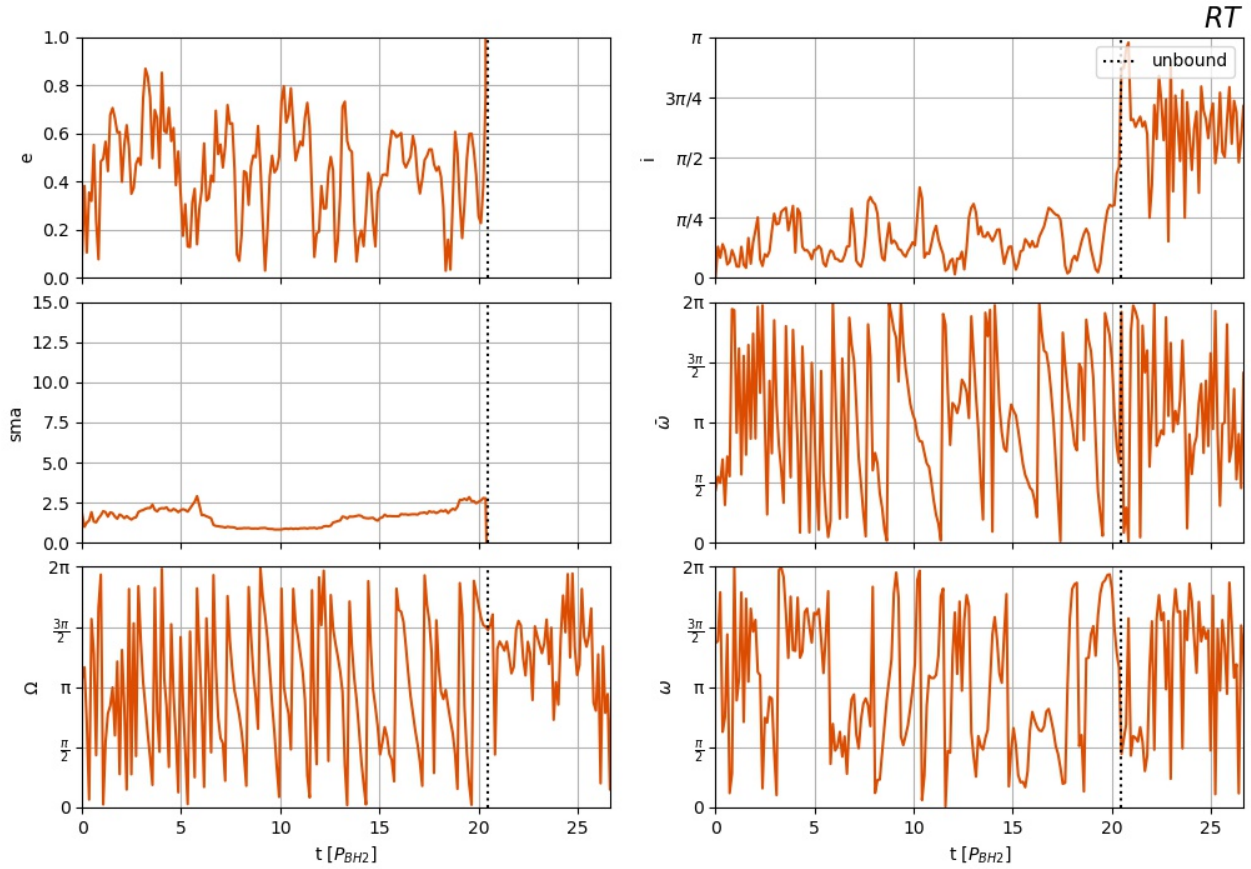

Figure 14. Kepler elements of one unbound particle for the RT simulation. The plots are the same Kepler elements as described in 10, but the black dashed vertical line shows where the particle becomes unbound. Note: After the star unbinds from BH1 the orbital elements can be ignored.

lost in the disk by limiting the magnitude of the gravitational force encountered between objects during our simulations.

We initialized all our simulations as in Figure 3 with a stellar disk and black hole companion meeting specific criteria that can be found in Table 1. The companions of the RT and T simulations prove too effective at unbinding stars in their disks, Figures 13, 14, and 15, and that the RT and T disks did not form an END when observing the individual and average unit eccentricity vectors, Figures 4, 5, 7, 8, and 9. Since the RT and T disks lost most of their mass, efficient two-body relaxation dampened the disks' precession rates and spread the disks out, Figure 10 and 11, so the simulations no longer met the resonance condition by the end. We find that the RT simulation demonstrated only artificial signs of apsidal alignment due to the their low particle disks dropping out of the resonance condition with their companion, and hastening their two-body relaxation timescale. Although our initial theory did not foresee the dramatic disk mass loss, we have not excluded the ability for an END to form when disk mass loss is accounted for.

Even though the individual and averaged eccentricity vectors showed no strong evidence for apsidal alignment in the R simulation seen in Figures 4 and 9, BH_2 resonates with its disk forming an END as seen by the periodic oscillations in the longitude of periapsis, Figure 12. Further analysis of the R simulations disk evolution showed little disk mass lost, Figure 13, compared to its torqued counterparts.

Realistically, our simulations model systems where the number of particles in a disk is on the order of millions. Additionally, our setup of two black holes, one of which has a circular flat stellar disk, views these systems as if BH_2 orbits around BH_1 and its disk, Figure 3. The initial simulation setup is true in the case of the R simulation, but for the RT and T simulations, the massive companions would actually create a binary black hole system where the two

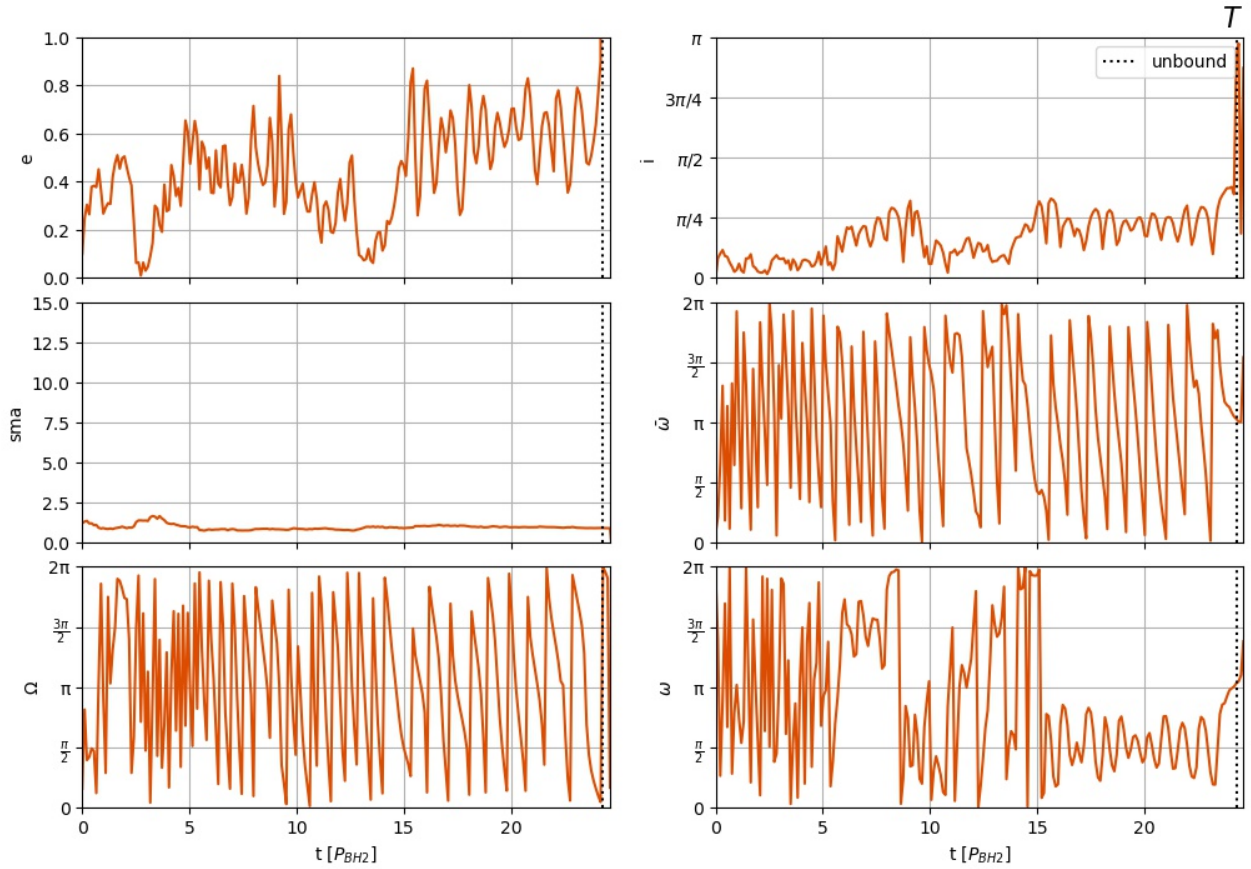

Figure 15. Kepler elements of one unbound particle for the T simulation.

black holes orbit one another while the stellar disk orbits BH_1. With this in mind, our results indicate that forming an eccentric nuclear disk in the presence of two black holes requires considerations for the amount of disk mass lost in the sufficiently torqued scenarios, and resonance with a companion alone creates apsidal alignment in a stellar disk.

5.1. *Future Work*

Future work includes testing END formation in disks with different initial distributions of eccentricities, inclinations, or semi-major axes. Simulating these systems with higher N would allow one to ultimately determine whether an END could form when the sufficient torque condition is met, but we would account for massive disk loss and two-body relaxation. Additionally, future research would compare the properties of BH_2 to its disks orbital elements ensuring BH_2 continues to satisfy the conditions it is initialized at, see 1. We would explore whether our systems causes unbound stars to be ripped apart, tidally disrupted, and how our torque and resonance conditions affect tidal disruption events. Finally, we would investigate the dynamical mechanisms related to eccentric dynamics and their affect on our models.

6. ACKNOWLEDGEMENTS

This work utilized resources from the University of Colorado Boulder Research Computing Group, which is supported by the National Science Foundation (awards ACI-1532235 and ACI-1532236), the University of Colorado Boulder, and Colorado State University. Additionally, this paper acknowledges the work and contributions of Tatsuya Akiba from JILA and Department of Astrophysical and Planetary Sciences, CU Boulder.

Software: `REBOUND` (Rein & Liu 2012)

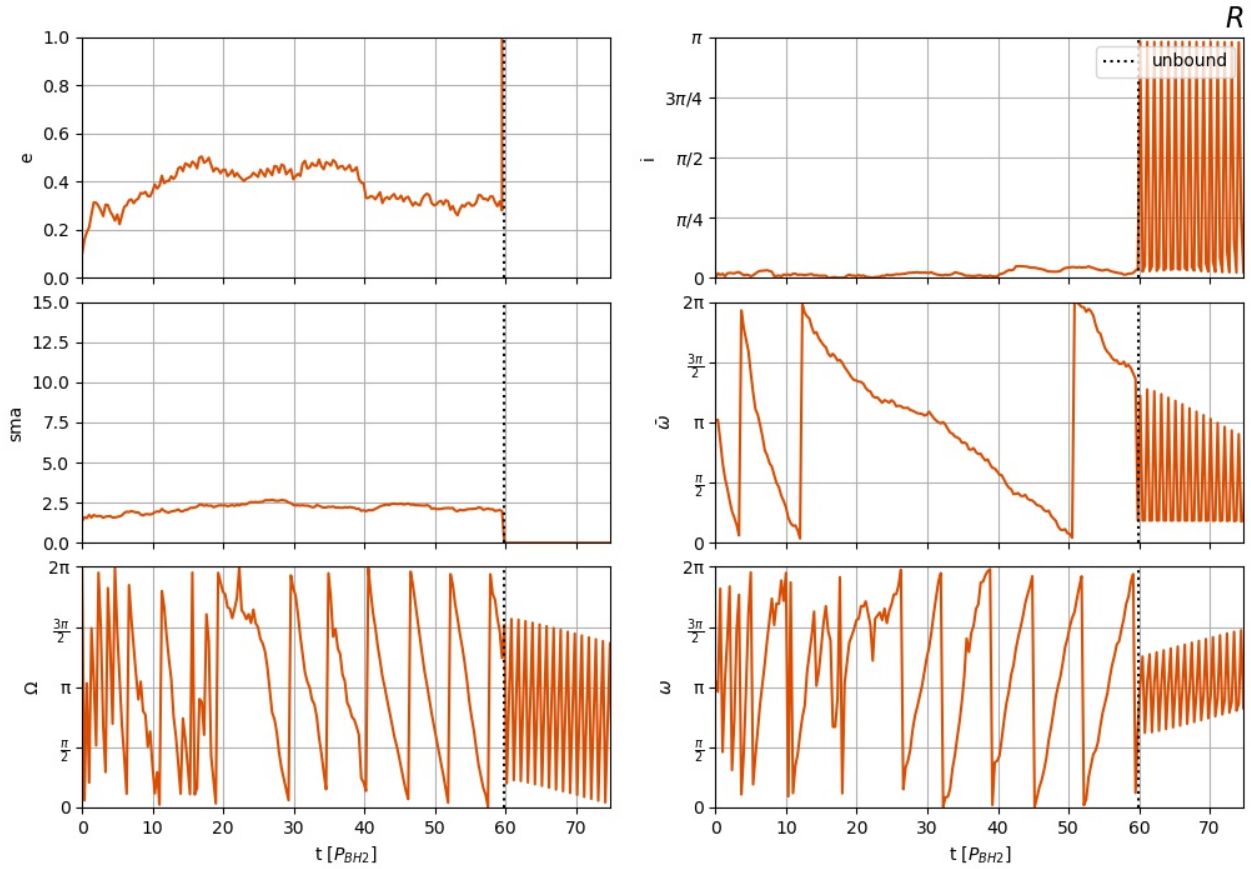

Figure 16. Kepler elements of one unbound particle for the R simulation.

APPENDIX

A. ORBITAL ELEMENTS

In astronomy one way to completely describe an orbit is to use Kepler orbital elements when discussing Keplerian orbits. First we define a reference direction, generally considered the positive x-axis with all angles in units of radians. The x-y plane is our reference plane, and we have the eccentricity, semi-major axis, inclination, the longitude of ascending node, argument of periapsis, and true anomaly to specify any orbit.

Looking at Figure 17 for reference, the eccentricity, e, tells us about the elongation, or the shape, of the orbit. Circular orbits have an eccentricity of zero, and highly elliptical orbits are near unity. Unbound orbits have eccentricities of one or greater. The distance from the center of an orbit to either the periapsis or apoapsis is called the semi-major axis, a. Now using Figure 18 we define the rest of the orbital elements.

The angle the orbit comes out of the reference plane is the inclination, i, and ranges from $[0, \pi]$. Another way to say that is the inclination tells us the orbiting direction and how the orbital plane tilts with respect to the reference plane. Counter-clockwise orbits in the reference plane define an inclination of zero. Alternatively, inclinations around π means the object orbits clockwise. Next, the point in an object's orbit where its orbital plane meets the reference plane on the orbit's ascent is the ascending node, ☊. The angle measuring the tilt over the minor axis, side-to-side, or the angle of the ascending node from the reference direction, gives us the longitude of ascending node, Ω, with values of $[0, 2\pi)$. The other ω also ranges from $[0, 2\pi)$, but represents the angle from the longitude of ascending node to the periapsis of the orbit, and so it is called the argument of periapsis. Lastly, the true anomaly, ν, defines where the object is on its orbit with respect to its periapsis, or the angle of the object's position from its eccentricity vector,

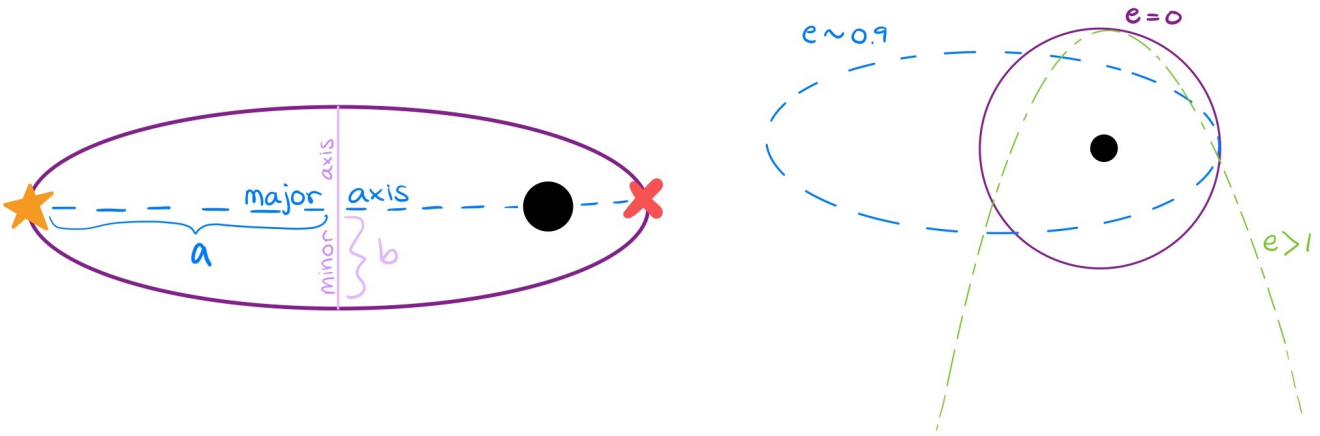

(a) Semi-major axis, a, of an eccentric orbit. (b) Orbits of various eccentricities.

Figure 17. (a) The axes of an orbit consist of the minor and major axis. The defined semi-major (half of major) axis, a, for an eccentric orbit. The semi-major axis can be described by, $a \propto b(1-e)^{-\frac{1}{2}}$.(b) Examples of orbits with eccentricities of zero (purple solid circle), near unity (blue dashed ellipse), and greater than unity, green dot-dash line. Figures created by author.

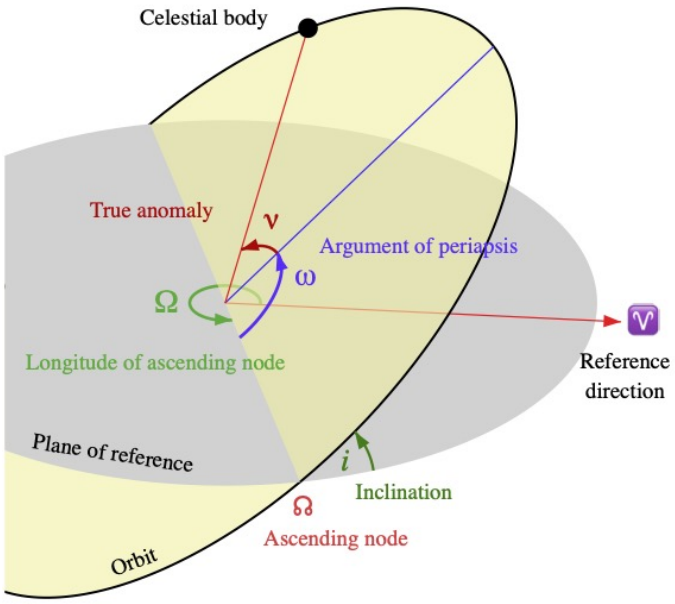

Figure 18. Shows the reference plane, orbital plane, inclination (i), longitude of ascending node(Ω), argument of periapsis (ω), and true anomaly (μ), for a given reference direction, (Υ). Figure taken from Wikipedia's Kepler Orbit page.

with angles from $[0, 2\pi)$.

For this paper we also use the angular momentum and eccentricity vectors to fully understand the dynamics in our simulations. As previously mentioned, the orbiting direction of an object is determined by the inclination which depends on its angular momentum, $\vec{J}$. The specific angular momentum, $\vec{J}$, is defined as the cross product (direction perpendicular to both) of the position and velocity vectors of an orbit, so $\vec{J} \approx \vec{r} \times \vec{v}$. The position vector, $\vec{r}$, points to the star from the central black hole, and the velocity vector, $\vec{v}$, points tangentially from the star in the direction of motion. Figure 19 shows an example of the aforementioned vectors, $\vec{J}, \vec{r}, \vec{v}, and\ \vec{e}$, for a star orbiting its central black hole counter-clockwise. Since we set up our disk in the x-y plane, our $+\hat{z}$ direction is our of the page. The compound

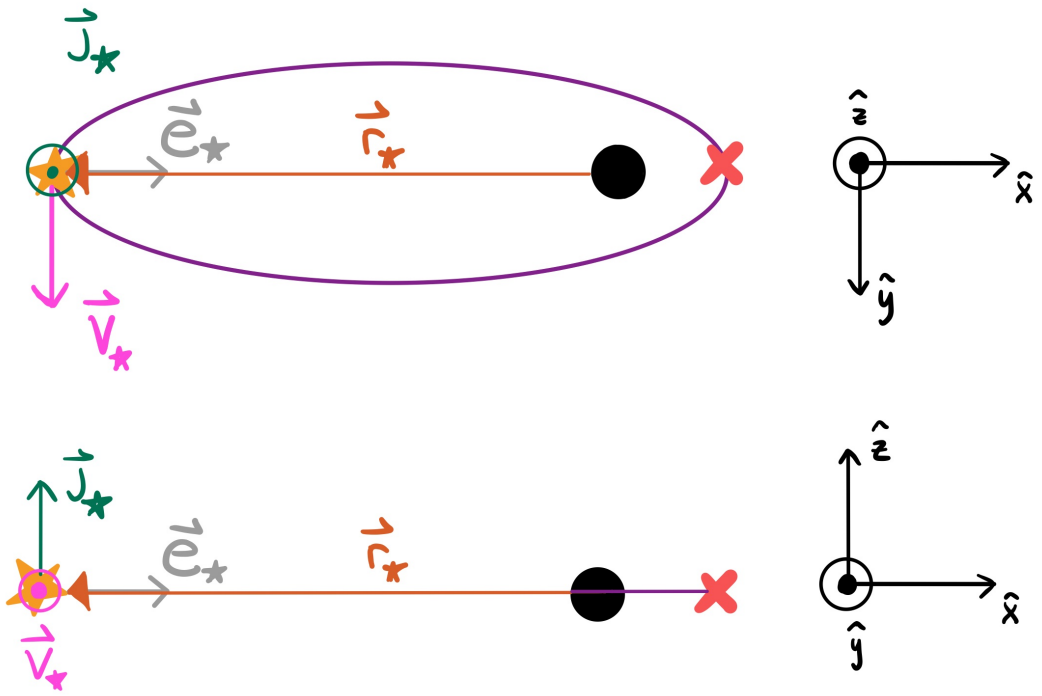

Figure 19. Drawing showing $\vec{J}, \vec{r}, \vec{v}, and \vec{e}$ for a star orbiting counter-clockwise around its central black hole with the defined axes shown to right of each image. The top figure shows a stellar orbit with all its vectors from above, x-y plane. While the bottom image shows the side view, x-z plane. Notice that $\vec{r_*}$ and $\vec{v_*}$ are perpendicular to one another in both images, so the corresponding $\vec{J}_*$ (using the right-hand rule) point out of the page for the upper image, $+\hat{z}$, and up for the lower image. Also, $\vec{e_*}$ points from the apoapsis of its orbit to the periapsis. Figure created by author.

angle of the longitude of periapsis, ϖ (where $\varpi = \Omega + \omega$), defines the orientation of the eccentricity vector, $\vec{e}$, with respect to the reference direction.

B. EXAMPLE OF SIMULATION PARAMETERS THAT SATISFY TORQUE AND RESONANT CONDITIONS

We want to find the mass of BH_2 such that it satifies the torque and resonant conditions given $a_{\rm out} = 2$, $a_{\rm star} = 1$, $M_{\rm disk\ total} = \frac{1}{100}$, $M_1 = 1$. Equation 7 gives us:

$$\frac{8}{a_2^3} = \frac{10^{-4}}{1 + M_2}, \tag{B1}$$

and Equation 8 says:

$$\frac{1}{M_2} = 2\pi \cdot 10^2 \cdot \frac{1}{a_2^2},$$

which, when rearranged, gives:

$$M_2 = \frac{a_2^2}{2\pi \cdot 10^2} \tag{B2}$$

Substituting Equation B2 into Equation B1 and solving for a_2, we get:

$$a_2 \approx 132,$$

and, by back-substituting, a corresponding 2 mass of:

$$M_2 \approx 27.7.$$

REFERENCES

Gruzinov, A., Levin, Y., & Zhu, J. 2020, arXiv e-prints, arXiv:2007.08471. https://arxiv.org/abs/2007.08471

Lauer, T. R., Faber, S. M., Gebhardt, K., et al. 2005, AJ, 129, 2138, doi: 10.1086/429565

Madigan, A.-M., Halle, A., Moody, M., et al. 2018, ApJ, 853, 141, doi: 10.3847/1538-4357/aaa714

Rauch, K. P., & Tremaine, S. 1996, New Astronomy, 1, 149

Rein, H., & Liu, S.-F. 2012, A&A, 537, A128, doi: 10.1051/0004-6361/201118085

Rein, H., & Spiegel, D. S. 2015, MNRAS, 446, 1424, doi: 10.1093/mnras/stu2164

Thomasson, M., Donner, K. J., Sundelius, B., et al. 1989, A&A, 211, 25

Tremaine, S. 1995, AJ, 110, 628, doi: 10.1086/117548